

## Adding Adhesion to a Chemical Signaling Model for Somite Formation

Nicola J. Armstrong, Kevin J. Painter\*, Jonathan A. Sherratt

*Department of Mathematics and the Maxwell Institute for Mathematical Sciences, School of Mathematical and Computer Sciences, Heriot-Watt University, Edinburgh, EH14 4AS, UK*

Received: 24 September 2007 / Accepted: 30 July 2008 / Published online: 3 September 2008  
© Society for Mathematical Biology 2008

**Abstract** Somites are condensations of mesodermal cells that form along the two sides of the neural tube during early vertebrate development. They are one of the first instances of a periodic pattern, and give rise to repeated structures such as the vertebrae. A number of theories for the mechanisms underpinning somite formation have been proposed. For example, in the “clock and wavefront” model (Cooke and Zeeman in *J. Theor. Biol.* 58:455–476, 1976), a cellular oscillator coupled to a determination wave progressing along the anterior-posterior axis serves to group cells into a presumptive somite. More recently, a chemical signaling model has been developed and analyzed by Maini and coworkers (Collier et al. in *J. Theor. Biol.* 207:305–316, 2000; Schnell et al. in *C. R. Biol.* 325:179–189, 2002; McInerney et al. in *Math. Med. Biol.* 21:85–113, 2004), with equations for two chemical regulators with entrained dynamics. One of the chemicals is identified as a somitic factor, which is assumed to translate into a pattern of cellular aggregations via its effect on cell–cell adhesion. Here, the authors propose an extension to this model that includes an explicit equation for an adhesive cell population. They represent cell adhesion via an integral over the sensing region of the cell, based on a model developed previously for adhesion driven cell sorting (Armstrong et al. in *J. Theor. Biol.* 243:98–113, 2006). The expanded model is able to reproduce the observed pattern of cellular aggregates, but only under certain parameter restrictions. This provides a fuller understanding of the conditions required for the chemical model to be applicable. Moreover, a further extension of the model to include separate subpopulations of cells is able to reproduce the observed differentiation of the somite into separate anterior and posterior halves.

**Keywords** Somitogenesis · Cell adhesion · Mathematical model · Pattern formation

---

\*Corresponding author.

*E-mail addresses:* [nicola\\_j\\_armstrong@hotmail.com](mailto:nicola_j_armstrong@hotmail.com) (Nicola J. Armstrong), [painter@ma.hw.ac.uk](mailto:painter@ma.hw.ac.uk) (Kevin J. Painter), [jas@ma.hw.ac.uk](mailto:jas@ma.hw.ac.uk) (Jonathan A. Sherratt).

N.J. Armstrong was supported by a Doctoral Training Account Studentship from EPSRC. K.J. Painter and J.A. Sherratt were supported in part by Integrative Cancer Biology Program Grant CA113004 from the US National Institute of Health and in part by BBSRC grant BB/D019621/1 for the Centre for Systems Biology at Edinburgh.

## 1. Introduction

The transformation from a single fertilized cell into a complex differentiated multicellular organism is built upon a sequence of precisely coordinated and interconnected events. During segmentation, the embryo is divided into a number of discrete units, laying down a body plan for subsequent development. Segmentation in a number of organisms, including mammals, fish, and birds, proceeds through the formation of somites, repeating blocks of cells fashioned from two parallel bands of mesenchymal tissue, known as the presomitic mesoderm (PSM) (or paraxial mesoderm), that lie on either side of the developing neural tube. Each new pair of somites appears with clockwork precision (once every 90 minutes in the chick; see, for example, Primmitt et al., 1989) following alterations to the adhesive and migratory properties of cells at the anterior ends of the PSM, which give rise to an epithelialized block. Simultaneously, a flow of cells into the posterior end maintains the length of the PSM while shifting it down the anterior-posterior (AP) axis of the embryo (see Fig. 1). For a general review of somitogenesis, see Pourquié (2001) or Dubrulle and Pourquié (2004).

A number of genes have been identified with closely controlled spatial and temporal expression within the PSM. Expression of *l-fng* and *c-hairy1* exhibits cycles with a period equal to the formation time of one somite (Palmeirim et al., 1997; McGrew et al., 1998). The cycling phase corresponds with position along the AP axis, resulting in periodic expression waves that sweep up the length of the PSM (see Fig. 1). The cyclical expression of such genes has reinforced the long-held notion that an underlying segmental clock regulates the transformation of PSM cells into somites (Cooke and Zeeman, 1976; Dale and Pourquié, 2000). FGF8 is also tightly controlled (Dubrulle et al., 2001; Dubrulle and Pourquié, 2004b) with a posterior–anterior gradient in FGF8 protein established via *fgf8* mRNA degradation (Dubrulle and Pourquié, 2004b). As segmentation proceeds, this gradient moves posteriorly with the same speed as the PSM, fixing the relative position of signaling levels. The borders marking boundaries between somites can be observed by the expressions of various genes: for example, following its initial cyclical expression, *c-hairy1* is fixed to a thin stripe of cells in the posterior half of a future somite (Palmeirim et al., 1997, see Fig. 1). This shows that the anterior portion of the PSM becomes segmented into groups of committed cells several cycles prior to their manifestation as an epithelialized block.

The transformation from the loosely connected mesenchymal cells of the PSM into an epithelialised somite requires alterations in the adhesive properties of the cells and extracellular matrix (ECM). The compaction of cells is believed to arise through an increase in cell adhesion (Cheney and Lash, 1984), and several studies have demonstrated roles for various classes of adhesion molecules including fibronectin (e.g., Ostrovsky et al., 1983; Lash et al., 1987; Duband et al., 1987) and cadherins (e.g., Hatta et al., 1987; Duband et al., 1987; Takeichi, 1988; Linask et al., 1998). Prior to and during their formation, somites become subdivided into distinct anterior and posterior portions (Saga and Takeda, 2001; Pourquié, 2001), a division necessary in their subsequent differentiation (Bagnall et al., 1989). One possibility is that differential cell–cell adhesion assists in the sorting and maintenance of the somite into these anterior and posterior compartments (Stern and Keynes, 1987), a notion reinforced by the distribution of various members of the cadherin family in the developing somite (e.g., Duband et al., 1987; Kimura et al., 1995; Horikawa et al., 1999).

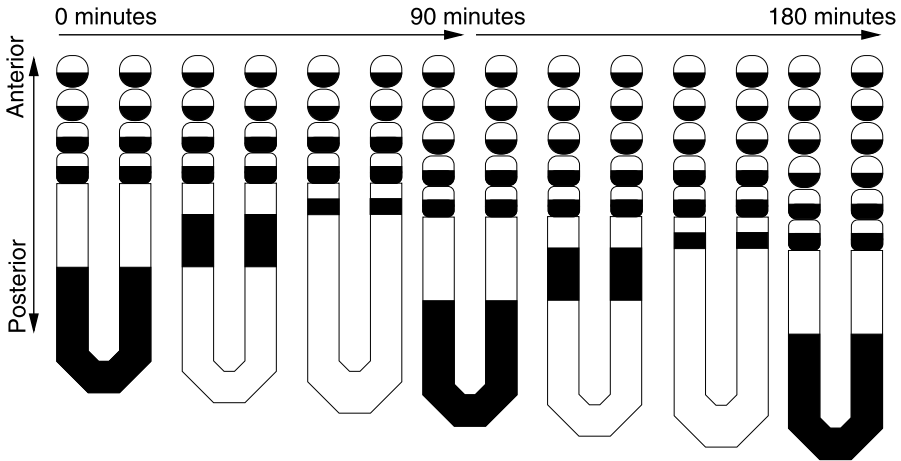


**Fig. 1** Schematic illustration of chick somitogenesis over a 2-somite timespan. As the PSM shifts posteriorly, groups of cells pinch from the anterior end to form somites. A number of genes display rhythmic gene expression throughout somitogenesis, for example, that of *c-hairy1* (black shading), which sweeps up the PSM as a wave of expression before fixing to the posterior half of a presumptive somite.

The metronomic advance of somitogenesis has positioned it as a leading case study for embryonic pattern formation, and a variety of theoretical models have been proposed to explain its mechanistic basis (see the reviews in Baker et al. 2006a, 2008; Kulesa et al., 2007). A number of these models posit that somites form through the interaction between a “clock” and a “wavefront” (Cooke and Zeeman, 1976), in which a cellular oscillator coupled with a wave of cellular determination along the AP axis of the PSM gates groups of cells into a presumptive somite. Recent molecular evidence has supported this theory: the graded FGF8 signaling has the characteristics required for the wavefront, while there is growing evidence for the components of a segmentation clock controlling the cyclical expression of genes such as *l-fng* and *c-hairy1* (Lewis and Ozbudak, 2007).

In the cell-cycle model proposed by Stern and coworkers (Stern et al., 1988; Primm et al. 1988, 1989), the “clock” is the cell-cycle: it is assumed that cells synchronize their cycle as they enter the PSM, and that somites develop later from groups of cells in the same phase. A mathematical formulation of this model has been derived by Maini and coworkers (Collier et al., 2000; Schnell et al., 2002; McInerney et al., 2004) which predicts normal somite formation and in addition accounts for abnormalities arising from specific “heat-shock” experiments. Yet the expression patterns of *l-fng* and *c-hairy1* argue against the cell-cycle acting as a segmental clock: while *l-fng* and *c-hairy1* expression oscillates with periods corresponding to the formation of one somite (approximately 90 minutes in the chick), about 6 somites form during a one cell-cycle for chick PSM cells. Therefore, the cell-cycle model of Stern and coworkers is debatable. Nevertheless, the mathematical model of Collier et al. (2000) is generic and does not depend crucially on the cell-cycle acting as the clock. At its simplest interpretation, it models a process in which periodic signaling bursts (determined by a clock) commit groups of activated cells (determined by a wavefront) into each somite. As such, the basic framework in Collier et

al. (2000) has been reinterpreted and extended (e.g., Baker et al. 2006a, 2006b) to account for more recent findings on the molecular control of somitogenesis.

While these models successfully demonstrate the partitioning of the PSM into prospective somites, there has been less focus either on the cellular movements or on pattern formation within somites. A reaction-diffusion based model proposed by Meinhardt (1986) partially addresses the latter: while it provides only a chemical prepattern, the model does capture AP patterning. The shaping of the somite through cellular movements has been considered in Schnell et al. (2002), who extended the model of Collier et al. (2000) by hypothesizing that the signaling factor acts as a chemotactic factor for cells. This work demonstrated aggregation of PSM cells into a somite; however, evidence for a chemotactic factor in somitogenesis is currently lacking. A recent model by Grima and Schnell (2007) has represented adhesive-driven somite formation through energy minimization of cell surface tension. While this model demonstrates the compaction of somitic cells into a ball, the regulation of adhesion through a chemical prepattern and the anterior-posterior division of somites was not addressed. Finally, Glazier et al. (2008) have proposed a computational model of the way in which adhesive and repulsive forces between cells conspire to generate somites; this model does not incorporate the origin of somite-cycle timing.

In this paper, we extend the chemical model of Collier et al. (2000) to explicitly include cellular dynamics. Our model assumes that a somite develops following up-regulation in the adhesive strength between the cells forming a presumptive somite. We show that the expanded model recreates the formation of somites in both one and two dimensions, but only under specific parameter constraints. Moreover, by extending the model to include distinct subpopulations of cells with differential adhesion properties, the model predicts the observed further differentiation of the somite into distinct anterior and posterior halves.

## 2. The chemical model

We begin by summarizing the chemical model originally proposed by Collier et al. (2000). As mentioned above, later efforts (e.g., Baker et al. 2006a; 2006b) modified and extended this work to account for limitations of the earlier model. Here, the focus is on the subsequent cellular dynamics rather than initial portioning of the paraxial mesoderm and we employ the simpler formulation of Collier et al. (2000). In this model, a somitic factor  $u(x, t)$  interacts with a signaling factor  $v(x, t)$  as follows

$$\begin{aligned}\frac{\partial u}{\partial t} &= \frac{(u + \mu v)^2}{\gamma + \rho u^2} \chi_u(x, t) - \nu u, \\ \frac{\partial v}{\partial t} &= \frac{\kappa \chi_v(x, t)}{\epsilon + u} - \lambda v + D \frac{\partial^2 v}{\partial x^2},\end{aligned}$$

where

$$\chi_u(x, t) = H(ct - x + x_1) \quad \text{and} \quad \chi_v(x, t) = H(ct - x + x_2).$$

Here  $t$  denotes time and  $x$  denotes space, measured in the anterior to posterior direction, with  $x = 0$  being the anterior end of the PSM at time  $t = 0$ . The Heaviside function,  $H$  has the form,

$$H(\alpha - x) = \begin{cases} 1 & \text{if } x \leq \alpha, \\ 0 & \text{if } x > \alpha, \end{cases}$$

while  $\mu, \gamma, \rho, \nu, \kappa, \epsilon, \lambda, D, c, x_1$ , and  $x_2$  are positive constants with  $x_1 > x_2$ . Nondimensionalization of this model (McInerney et al., 2004<sup>1</sup>) can be performed by setting

$$\begin{aligned} \hat{t} &= \lambda t, & \hat{x} &= \frac{x}{(x_1 - x_2)}, & \hat{u} &= \rho \nu u, & \hat{v} &= \rho \nu u, \\ \hat{v} &= \frac{\lambda}{\kappa \nu \rho} v, & \hat{\mu} &= \frac{\mu \kappa \nu^2 \rho^2}{\lambda}, & \hat{\gamma} &= \gamma \lambda \nu \rho, \\ \hat{\kappa} &= \frac{\lambda}{\nu}, & \hat{\epsilon} &= \epsilon \nu \rho, & \hat{D} &= \frac{D}{\lambda (x_1 - x_2)^2}, \\ \hat{c} &= \frac{c}{\lambda (x_1 - x_2)}, & \hat{x}_1 &= \frac{x_1}{x_1 - x_2}, & \hat{x}_2 &= \frac{x_2}{x_1 - x_2}, \end{aligned} \quad (1)$$

to derive (dropping the ‘‘hats’’)

$$\frac{\partial u}{\partial t} = \frac{(u + \mu v)^2}{\gamma + \kappa u^2} \chi_u(x, t) - \frac{u}{\kappa}, \quad (2a)$$

$$\frac{\partial v}{\partial t} = \frac{\chi_v(x, t)}{\epsilon + u} - v + D \frac{\partial^2 v}{\partial x^2}, \quad (2b)$$

where

$$\chi_u(x, t) = H(ct - x + x_1) \quad \text{and} \quad \chi_v(x, t) = H(ct - x + x_2).$$

Note that following the nondimensionalization  $x_1 - x_2 = 1$ .

Intuitively, the above model generates somites as follows: the Heaviside functions  $\chi_u$  and  $\chi_v$  progress posteriorly along the PSM with constant speed  $c$  (modeling the action of a ‘‘wavefront’’). As  $\chi_v$  becomes active, regions of low  $u$  ( $u \approx 0$ ) observe rapid production of the signalling factor leading to a diffusive pulse centered on  $x_2 + ct$ . The increase in  $v$  leads to a corresponding increase in the somitic factor up to the point  $x_1 + ct$ . Under certain parameter constraints (discussed in detail in McInerney et al., 2004), the model gives rise to periodic step-changes in the concentration of  $u$ . A reproduction of the results of this model is presented in Fig. 2 using parameter values and the following initial conditions from McInerney et al. (2004):

$$u(x, 0) = \begin{cases} 1 & \text{if } x < 0, \\ 0 & \text{otherwise,} \end{cases} \quad (3a)$$

$$v(x, 0) = H(-x) + A \cosh(\lambda(10 - |x|)), \quad \text{where}$$

<sup>1</sup>The actual rescalings given on p. 91 of McInerney et al. (2004) contain a typographical error: there is a ‘‘ $\nu$ ’’ in the denominator of the expression for  $\hat{c}$ , which should be ‘‘ $\lambda$ .’’

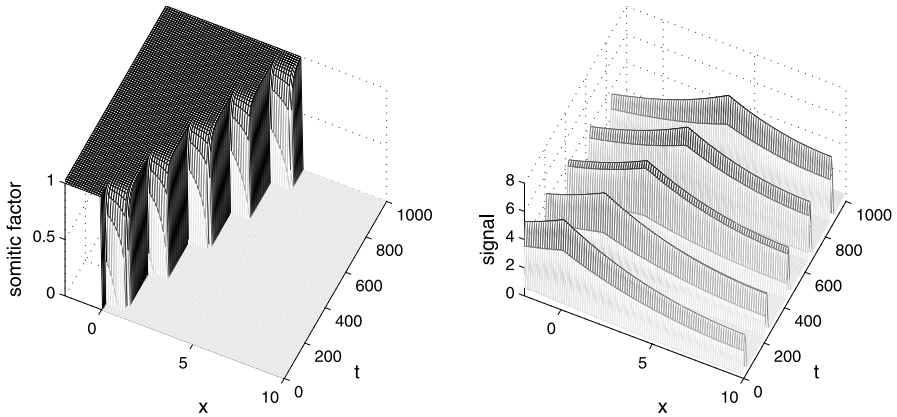


**Fig. 2** Numerical results of the chemical model (2) of somitogenesis showing five successive step-changes in the somitic factor  $u$ , each of which is interpreted as the initiation event for the formation of a somite. The solutions for  $u$  (left panel) and  $v$  (right panel) are shown from  $t = 0$  to  $t = 1,000$ . Initial conditions and parameter values were taken from McInerney et al. (2004); specifically we used (3) at  $t = 0$  and took  $\mu = 10^{-4}$ ,  $\gamma = 10^{-2}$ ,  $\kappa = 10$ ,  $c = 5 \times 10^{-3}$ ,  $\epsilon = 10^{-3}$  and  $D = 50$ . The equations were solved numerically as described in the Appendix, on the domain  $-10 < x < 10$  (only the relevant part of the domain is plotted) subject to zero flux boundary conditions, with  $\Delta x = 0.0125$ .

$$A \equiv \frac{\text{sign}(x)}{2 \cosh(10\lambda)}, \quad \lambda \equiv \sqrt{\frac{1}{50}}. \quad (3b)$$

### 3. An expanded model with an adhesive cell population

Our objective in this paper is to investigate the potential for the model (2) to induce aggregations in an adhesive cell population in a manner comparable with actual somite formation. To do this, we augment the model (2) with an additional equation for adhesive cells. We deliberately assume that there is no feedback from changes in cell density into the chemical equations; this would be a natural area for future study, but our aim here is to leave the chemical model in its existing and well-studied form, and to draw precise conclusions on its implications for cell aggregation due to changes in adhesion.

Our model for an adhesive cell population is based directly on the work of Armstrong et al. (2006), which we now summarize. The model consists of an integro-advection-diffusion equation in which the integral represents the effect of adhesion between cells on their movement:

$$\frac{\partial n(x, t)}{\partial t} = \overbrace{D_n \frac{\partial^2 n(x, t)}{\partial x^2}}^{\text{Diffusion}} - \underbrace{\frac{\alpha \phi}{R} \frac{\partial}{\partial x} \left[ n(x, t) \int_{-R}^R f(n(x + x_0, t)) \omega(x_0) dx_0 \right]}_{\text{Adhesion}}. \quad (4)$$

Here,  $n(x, t)$  is the cell density at position  $x$  and time  $t$ .  $D_n$ ,  $\alpha$ ,  $\phi$ , and  $R$  are positive constants, a full description of which can be found in Armstrong et al. (2006). In brief,  $D_n$  is the diffusion coefficient,  $\alpha$  is the adhesion coefficient,  $\phi$  relates to the viscosity of the cells, and  $R$  describes the radius over which cells can sense their surroundings. The function  $f(n)$  represents the attractive adhesive force between the cells. Force will increase with cell density when this is small, but will decrease at higher cell densities, as close-packing is approached; Armstrong et al. (2006) take  $f(n) = n(2 - n/N_{\max})$  as a simple function with an appropriate qualitative form.

The function  $\omega(\cdot)$  represents the variation in adhesive force over the sensing region of the cell; for uniqueness, we impose the condition  $\int_0^R \omega(x_0) dx_0 = 1$ . There is a natural constraint that  $\omega(\cdot)$  is odd, since adhesive forces will always be directed toward cell centers, but otherwise there is no data that we are aware of on which  $\omega(\cdot)$  can be based. Armstrong et al. (2006) take  $\omega(x_0) = \text{sign}(x_0)$  as their basic functional form, and we will do likewise.

Armstrong et al. (2006) showed that provided the adhesion coefficient  $\alpha$  is sufficiently large, Eq. (4) predicts the aggregation of an initially uniform cell population (with a small amount of noise) into discrete cell clusters, as has been demonstrated in a large number of *in vitro* experiments (see, for example, Steinberg, 1962; Foty and Steinberg 2004, 2005). The model has recently been applied to the invasive phase of solid tumour growth by Gerisch and Chaplain (2008).

To apply this adhesion model to somitogenesis, we assume that movement due to adhesion depends on both cell density and the concentration of the somitic factor, via the product  $n(x, t)u(x, t)$ . A dependence on  $u(x, t)$  ensures that only somitic cells move by adhesion, and similarly, we include the term  $u(x + x_0, t)$  inside the integral, which ensures that the adhesive movement is only influenced by other somitic cells. Effectively, this supposes an up-regulation in the strength of cell–cell adhesion in cells specified to form the next somite. This gives, in dimensional form, the equation for cell density as

$$\begin{aligned} \frac{\partial n(x, t)}{\partial t} = & \frac{\partial}{\partial x} \left[ D_n \frac{\partial n(x, t)}{\partial x} - \frac{\alpha \phi}{R} u(x, t) n(x, t) \right. \\ & \left. \times \int_{-R}^R u(x + x_0, t) f(n(x + x_0, t)) \omega(x_0) dx_0 \right]. \end{aligned} \quad (5)$$

Equation (5) can be nondimensionalized using the scalings employed in the chemical model,  $\hat{t} = \lambda t$ ,  $\hat{x} = x/(x_1 - x_2)$ ,  $\hat{u} = \nu \rho u$ , and a scaling on the cell density  $\hat{n} = n/N_{\max}$ . Introducing new parameters

$$\hat{D}_n = \frac{D_n}{\lambda(x_1 - x_2)^2}, \quad r = \frac{R}{x_1 - x_2} \quad \text{and} \quad \hat{\alpha} = \frac{\alpha \phi v^2 \rho^2 N}{\lambda R(x_1 - x_2)},$$

dropping the ‘‘hats’’ for notational convenience, and taking  $f(n) = n(2 - n)$ , we obtain the nondimensional form of the cell equation as

$$\begin{aligned} \frac{\partial n(x, t)}{\partial t} = & \frac{\partial}{\partial x} \left[ D_n \frac{\partial n(x, t)}{\partial x} \right. \\ & \left. - \alpha u(x, t) n(x, t) \int_{-r}^r u(x + x_0, t) n(x + x_0, t) \right] \end{aligned}$$

$$\times (2 - n(x + x_0, t))\omega(x_0) dx_0 \Big]. \quad (6)$$

Our expanded model consists of this equation together with the chemical model (2), from which (6) is decoupled.

#### 4. Solutions of the expanded model

We solve the chemical model (2) and the cell equation (6) numerically, using the method described in the [Appendix](#). The chemical model is formulated on an infinite domain, with somites forming only in  $x > 0$ . Therefore, we assume that there are no potentially adhesive cells in  $x < 0$ , with an initial cell density in  $x > 0$  that is uniform except for a very small amount of noise. Thus, we take  $n = 0$  in  $x < 0$  and  $n = N + \Phi(x)$  in  $x > 0$ . Here,  $N$  is a new dimensionless parameter, with the constraint  $0 < N < 2$ , and  $\Phi(\cdot)$  is chosen randomly from a uniform distribution between  $\pm 5 \times 10^{-4}$ . The noise term  $\Phi(\cdot)$  has no significant effect on the solutions of (2, 6). However, it will play an important role when we extend the model to represent two cell populations (in Section 5), and we include it at this stage for consistency.

Our expanded model has four additional parameters that are not in the chemical model:  $D$ ,  $\alpha$ ,  $r$ , and  $N$ . There is no precise data on which any of these parameters can be based, but some rough estimates are possible. The cell diffusion coefficient can be expected to be 3–4 orders of magnitude less than that for the signaling molecule (which has  $D = 50$ ), and following Schnell et al. (2002), we take  $D_n = 0.02$ . For the cell sensing radius, the physical cell volume provides only a lower bound: motile cells change shape and extend protrusions (e.g., filopodia, lamellipodia) that could contribute to a substantially larger sensing range. We take  $25 \mu\text{m}$  as a reasonable estimate; the effects of varying  $R$  are discussed later in the paper (see Fig. 9). Since the dimensional wavelength of the somite pattern is about  $100 \mu\text{m}$  (in chick; see, for example, Dubrulle et al., 2001), the dimensionless sensing radius  $r$  will be about 0.25. For  $\alpha$  and  $N$ , a natural constraint arises from the wavelength of aggregates seen in the cell-only model (4): we can expect this to be about 1, in order to give a pattern of somites with the required wavelength of 1. Standard linear stability analysis for (4) implies that the growth rate  $\Lambda$  of small perturbations is related to their wave number  $k$  via the dispersion relation

$$\Lambda = -D_n k^2 - 4\alpha N(1 - N)(\cos(kr) - 1). \quad (7)$$

The fastest growing wave number,  $k_m$ , will satisfy  $\partial \Lambda / \partial k|_{k=k_m} = 0$ , giving

$$-k_m D_n + 2\alpha N(1 - N)r \sin(k_m r) = 0.$$

This condition can only be satisfied when  $k_m = 2\pi$  if  $r < 1/2$ . Biologically, this has the natural interpretation that the sensing radius of the cells must be less than half of the length of a somite; such a restriction is entirely expected. Provided that  $r < 1/2$ , the constraint  $2\pi/k_m \approx 1$  implies that the growth rate  $\Lambda$  is always positive and that approximately,

$$\alpha N(1 - N)r \sin(2\pi r) = \pi D_n. \quad (8)$$

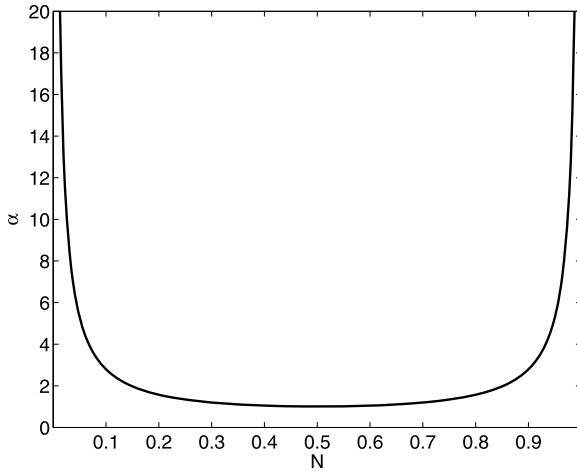


**Fig. 3** A plot of the adhesion coefficient,  $\alpha$ , as a function of the initial steady state population density,  $N$ , that is required to give a pattern of wavelength 1. The condition for this is given in (8), and is derived by requiring the most linearly unstable wave number to be  $2\pi$ . The other parameter values are  $D_n = 0.02$  and  $r = 0.25$ .

This condition is illustrated in Fig. 3 for  $D_n = 0.02$  and  $r = 0.25$ . Clearly, we require  $0 < N < 1$ . Moreover, the adhesion coefficient  $\alpha$  must be significantly greater than the diffusion coefficient. This creates difficulties for numerical solution of the equations, and the resolution of these is discussed in the [Appendix](#). Substituting  $k = 2\pi$  back into the dispersion relation (7) and using condition (8) yields a formula for the (dimensionless) doubling time  $\log 2/\Lambda$  with which patterns will initially develop from the uniform PSM:

$$T_{\text{doubling}} \equiv \frac{\log 2}{\Lambda} = \frac{\log 2}{4\pi^2 D} \left\{ \frac{\tan(\pi r)}{\pi r} - 1 \right\}^{-1}.$$

Reverting to dimensional quantities via (1) gives a dimensional doubling time of

$$T_{\text{doubling}}^{\text{dim}} = \frac{\log 2}{4\pi^2} \frac{(x_2 - x_1)^2}{D^{\text{dim}}} \left\{ \frac{\tan(\pi R)}{\pi R} - 1 \right\}^{-1}.$$

Recall that  $(x_2 - x_1)$  is the width of one somite, which is a known quantity; however, the dimensional cell sensing radius  $R$  and the dimensional value  $D^{\text{dim}}$  of the signaling factor diffusion coefficient are currently unknown; the value of the latter is particularly uncertain. Accurate estimates of these parameters would enable quantitative comparison of model predictions and experimental data on aggregation rates.

We solved (2) and (6) numerically for a wide range of pairs  $\alpha, N$  satisfying the approximate constraint (8), with  $D = 0.02$  and  $r = 0.25$ , and with the chemical parameters in (2) taken from McInerney et al. (2004) (listed in the legend of Fig. 2). In an intensive program of simulations, we were unable to find values of  $\alpha$  and  $N$  giving cellular aggregations with the required spacing of about 1. Rather, cells do aggregate, but these aggregations coalesce. A typical example is shown in Fig. 4: at  $t = 500$ , three wavefronts

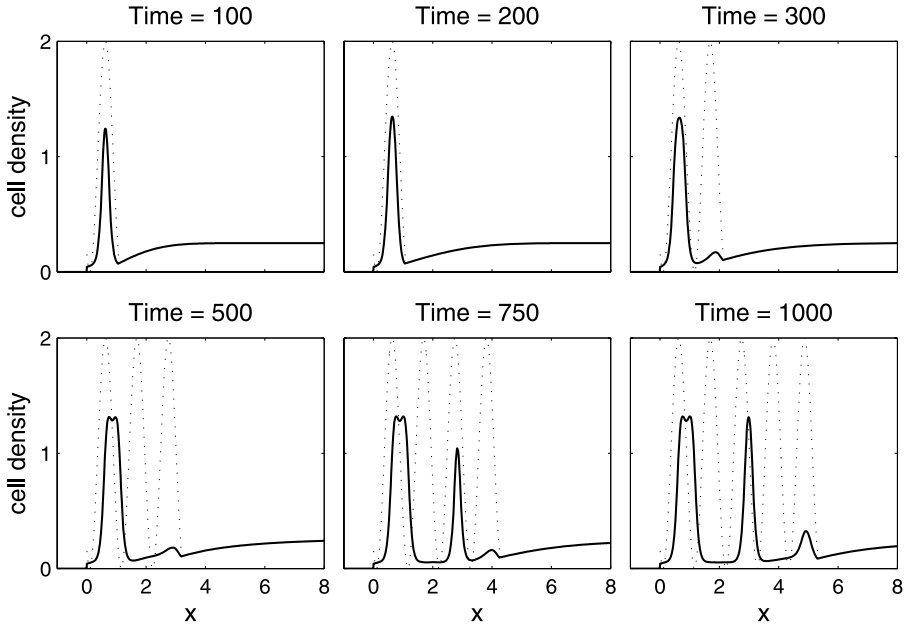


**Fig. 4** Numerical results of the expanded model (2, 6). The cell parameters are  $D = 0.02$ ,  $\alpha = 1.34$ ,  $N = 0.25$ , and  $r = 0.25$ , which satisfy (8). The chemical parameters are as in Fig. 2. The solid line shows the cell density profile at intervals between  $t = 0$  to  $t = 1,000$ , while the dotted line shows the positions where we expect somites to form, as predicted by the corresponding advance of the somitic factor wavefront (see Fig. 2). The initial conditions are  $n = 0$  in  $x < 0$  and  $n = N + \Phi(x)$  in  $x > 0$ , where  $\Phi(\cdot)$  is a small level of noise that is added at each grid element in the numerical scheme; we choose  $\Phi(\cdot)$  randomly from a uniform distribution between  $\pm 5 \times 10^{-4}$ . The equations were solved numerically as described in the Appendix, on the domain  $-10 < x < 10$  subject to zero flux boundary conditions (only the relevant part of the domain is plotted) with  $\Delta x = 0.0125$ .

of somitic factor have occurred, yet the cells have grouped into one large aggregate instead of three distinct peaks. At later times, new aggregates do form, but with a different wavelength to the underlying chemical model. A possible explanation for this may be that the pattern of wavelength about 1 is not stable on the timescale of somite formation in the model, and we now consider this further.

#### 4.1. Pattern stability and the speed of somite formation

To investigate further our failure to find patterns of an appropriate wavelength, we consider the cell-only model given by setting  $u \equiv 1$  in (6). Again, fixing  $D = 0.02$  and  $r = 0.25$ , with  $\alpha$  and  $N$  satisfying (8), numerical solutions show that small perturbations of a uniform cell population do initially generate a pattern of aggregations with wavelength about 1, but that this pattern rapidly coarsens, giving a much longer wavelength (Fig. 5). Such coarsening is a well-documented phenomenon in models with directed cell movement and no kinetics (e.g., Hillen and Painter, 2001).

These results suggest that the required pattern wavelength of about 1 might be recovered if we increase the dimensionless speed at which the pattern travels down the

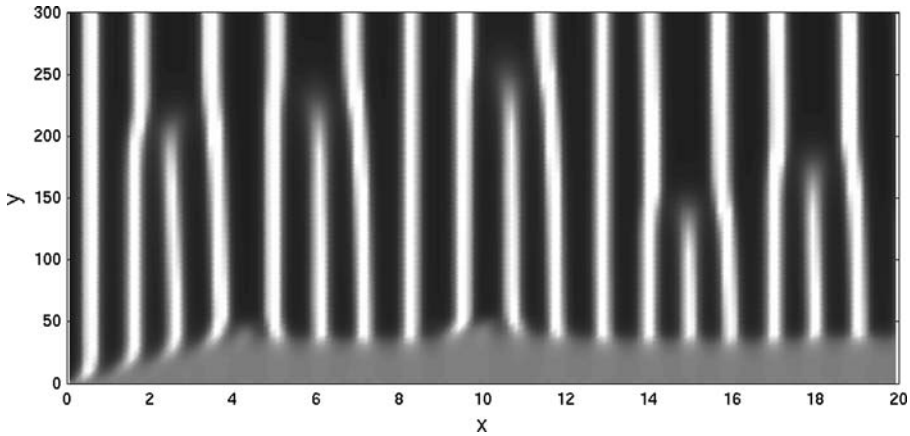


**Fig. 5** Numerical results of the cell-only model given by setting  $u \equiv 1$  in (6). The parameters are  $D = 0.02$ ,  $\alpha = 1.34$ ,  $N = 0.25$ , and  $r = 0.25$ , which satisfy (8). Therefore, linear stability analysis predicts a pattern of wavelength 1. This wavelength does develop initially, but coarsening of the pattern occurs over about 100 dimensionless time units. This is comparable with the timescale of somite formation in the cell cycle model for the parameters used by McNerney et al. (2004), which imply a dimensionless time interval of 200 between the formation of successive somites. Cell density is indicated by greyscale shading (black = low, white = high). The equations were solved numerically as described in the Appendix, on the domain  $0 < x < 20$ , subject to zero flux boundary conditions with  $\Delta x = 0.0125$ .

presomitic mesoderm. The dimensional value of this speed is known (about  $0.02 \mu\text{m s}^{-1}$  in chick (Primmett et al., 1989; Dubrulle et al., 2001)), but the corresponding dimensionless value depends on the decay rate of the signaling factor, which is unknown. In Fig. 4, we have followed McNerney et al. (2004) and used  $c = 5 \times 10^{-3}$ , which corresponds to a half life of 17 s for the signaling factor. However, Collier et al. (2000) and Schnell et al. (2002) use the larger value  $c = 5 \times 10^{-2}$ , which implies a signaling factor half life of 2.8 min. In Fig. 6, we show numerical solutions of (2, 6) with this larger value of  $c$ ; the other cell cycle model parameters are as in Fig. 4, and we vary  $N$  with  $\alpha$  determined by (8). For initial cell densities  $N$  less than about 0.6, the faster patterning speed allows somites of the required wavelength to form. Simulations indicate that the somites remain stable over a long-time interval: an animation for the  $N = 0.3$  case is available at <http://www.ma.hw.ac.uk/~painter/somites/movie.html>, showing the formation of 18 somites (corresponding to 27 hours in the chick). However, in the case of higher initial densities ( $N \geq 0.7$ ), the aggregations still tend to coalesce: coarsening occurs more quickly as  $N$  increases. A pattern of wavelength approximately 1 can be recovered by further increasing the speed  $c$ , in order that somites form before coarsening occurs. However, if the speed becomes too great, the chemical model does not give solutions of a form that corresponds to somite formation, and hence (6) does not show patterning of an appropriate form (illustrated in Fig. 7). In this case, successive pulses of the signaling molecule  $v$  occur too rapidly to allow distinct transitions in the somitic factor  $u$ ; rather, these transitions merge to give a gradual increase in  $u$ , spreading across the domain.

Figure 8 illustrates schematically the constraints on the wave speed. There is an upper bound on the speed, which is governed by the chemical model (2). This is the speed beyond which distinct wavefronts of the somitic factor are no longer observed. The lower

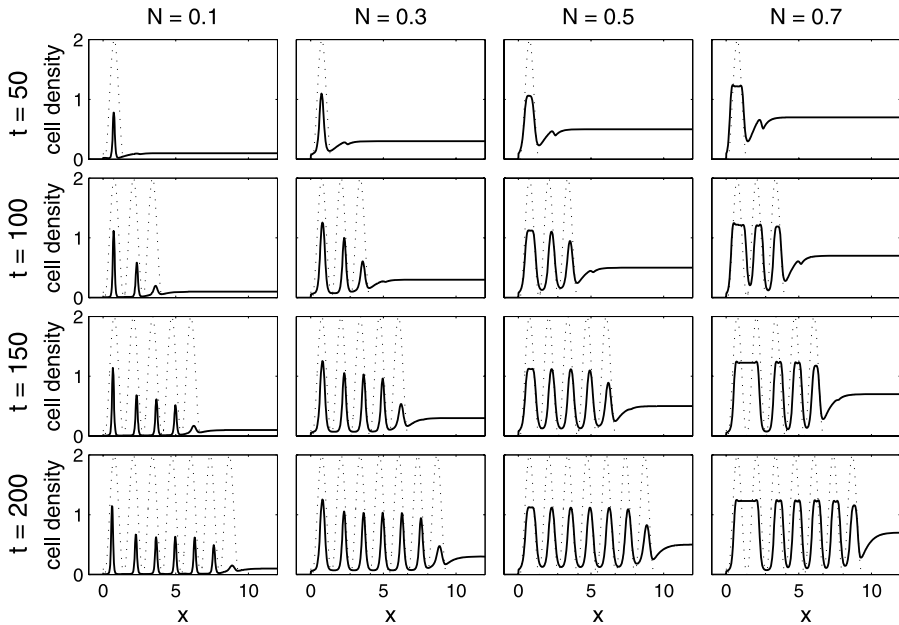


**Fig. 6** Solution profiles at  $t = 50, 100, 150,$  and  $200$  for the expanded model (2, 6), with the speed of pattern formation  $c$  faster than in Fig. 4. We use  $c = 5 \times 10^{-2}$ , and vary the initial cell density  $N$  while  $\alpha$  is determined by (8). Other parameters are as in Fig. 4. With this higher value of  $c$ , coarsening does not occur on the timescale of somite patterning for  $N$  less than about 0.6, and the model predicts a pattern of cellular aggregations with wavelength about 1, corresponding to somite formation. However, for larger values of  $N$ , coarsening occurs more quickly and the cell aggregations coalesce. The equations are solved for  $-10 < x < 20$  with initial conditions and numerical details as described in Fig. 4. An animation over a longer time interval and on a larger domain ( $-10 < x < 30$ ) for the  $N = 0.3$  case is available at <http://www.ma.hw.ac.uk/~painter/somites/movie.html>.

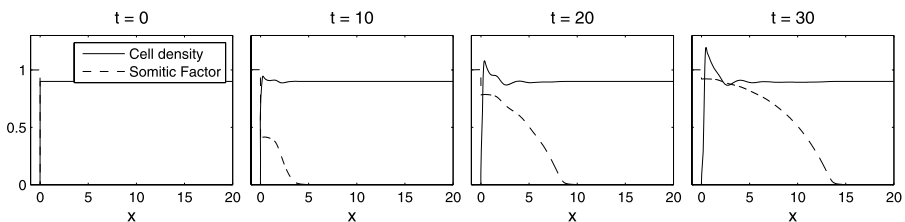


**Fig. 7** A solution of the model equations (2, 6) when the pattern formation speed  $c$  is too high for somite formation. The parameter values are as in Fig. 6, but with  $N = 0.9$  and  $c = 0.5$ . For such a high value of  $c$ , the chemical model loses the distinct steps in somitic factor concentration that characterize somite formation; instead, there is simply a wave of somitic factor progressing steadily across the domain. The cell aggregations that start to form are not a function of changes in the somitic factor level; rather they reflect the intrinsic tendency of an adhesive cell population to aggregate. Thus, essentially the same solution would develop in the cell-only model (4). The initial conditions and numerical details are as in Fig. 6.

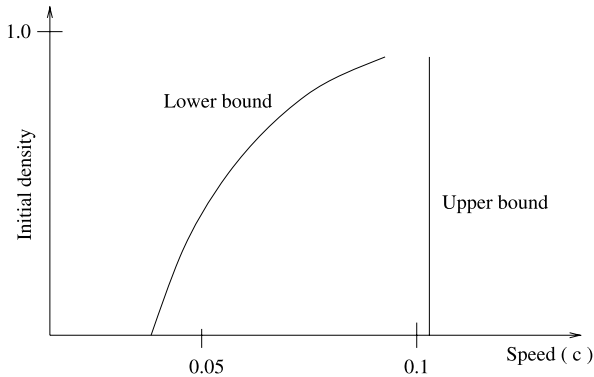


**Fig. 8** A schematic illustration of the upper and lower bounds on the speed parameter,  $c$ , as a function of initial density,  $N$ , for the model (2, 6) to predict somite formation. The numerical values are based on simulations, but the development of an appropriate pattern is not a precise condition, and hence the bounds are not precise.

bound is governed by the cell equation (6) and is the speed at which somite formation becomes faster than the coarsening process. This speed depends on the initial population density. Somites are able to form when the combination of initial cell density and pattern formation speed lie between these two bounds; the range becomes more narrow as the initial cell density increases. Within this range, the model predicts that somite size increases with the wave speed (results omitted for brevity). This is in agreement with experimental results on the modification of somite patterning by implantation of heparin beads soaked in the signaling molecule FGF8 (Dubrulle et al., 2001), and with the predictions of an extended version of the chemical model that includes an equation for FGF8 (Baker et al. 2006a, 2006b). It should be noted that Fig. 8 is schematic: the numerical values are based on simulations, but the development of an appropriate pattern is not a precise condition, and hence the bounds are not precise.

In the simulations of Fig. 6, the time between specification of the chemical pattern and formation of physical somites is about that taken for one somite to form, which corresponds to about 90 minutes in the chick. In contrast, the experimental data of Dubrulle et al. (2001) on the regulation of somite formation by FGF8 imply a delay of about 9 hours (also in chick). A natural explanation for this discrepancy is that the “somitic factor” is not itself an adhesion molecule, but rather the first stage in a sequence of chemical signals that leads to adhesion molecule expression (see Glazier et al., 2008). Alternatively, it is worth noting that there is little concrete data by which parameters of the cell equation (6) can be set: in the simulations here,  $D_n = 0.02$  (based on the value used in Schnell et al., 2002) and  $r = 0.25$  while  $\alpha$  and  $N$  were constrained through (8). To determine the sensitivity of the patterning to the cell parameters, each of  $D_n$  and  $\alpha$  were decreased by a factor of 10. Comparing the top and middle rows in Fig. 9, we find that the rate at which somites form is greatly reduced while their positioning/spacing is unaffected: thus, the time between specification and actual somite formation may partly be explained simply through slower cell movement. The sensitivity to the sampling radius was examined by performing a simulation with  $r = 0.1$  (a dimensional sampling radius of 10  $\mu\text{m}$ ),  $D_n = 0.02$ ,  $N = 0.3$  with  $\alpha$  determined by (8). Somites again develop at their predicted positions (Fig. 9, bottom

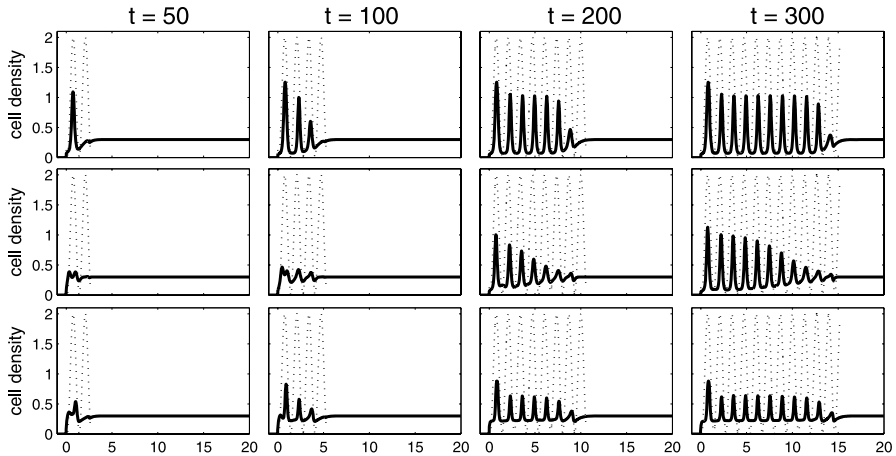


**Fig. 9** Solutions to the model equations (2, 6) illustrating the effects of changes to cell-equation parameters. Solid lines plot the cell density at the indicated times while the dotted lines indicate the expected positions of the somites, as predicted by the step-changes of the somitic factor. For all three rows, the parameters, initial conditions, and numerical details are as described in Fig. 6, except: top row,  $N = 0.3$ ,  $r = 0.25$ ,  $D_n = 0.02$ , and  $\alpha$  determined by (8); middle row,  $N = 0.3$ ,  $r = 0.25$ ,  $D_n = 0.002$ , and  $\alpha$  determined from (8); bottom row,  $N = 0.3$ ,  $r = 0.1$ ,  $D_n = 0.02$ , and  $\alpha$  determined from (8). Lower diffusion and adhesion coefficients result in a slower accumulation of cells into somites (middle row) while a smaller sampling radius decreases the maximum density of the aggregated cells. No change to the positioning of the somites is observed.

row), albeit with a reduced maximum density. Finally, cell movement was switched off in the PSM (thus pinning the cells) by introducing a somitic-factor dependent cell diffusion term. This generated the same qualitative behavior as above (data not shown).

#### 4.2. The size of the first somite

A consistent feature of our simulations of (2, 6) subject to (3) and  $n(x > 0, t = 0) = N$ ,  $n(x < 0, t = 0) = 0$  is that when a pattern corresponding to somite formation develops, the first somite is larger than the others (see, for example, Fig. 6). We hypothesize that this may be attributable to our choice of initial conditions, which mean that more cells are available to form the first somite than for later aggregations. To test this hypothesis, we solve the model again, choosing an initial distribution which increases smoothly from zero to  $N$  over the length of the first two somites. The results in this case can be seen in Fig. 10. With these initial conditions the first somite is of approximately the same size as later aggregations. This confirms that the increased size of the first somite in simulations such as those in Fig. 6 is simply due to the choice of initial conditions, which have the effect of amplifying the coarsening behavior near  $x = 0$ . Note that there is no precise experimental data on which initial conditions can be based.

#### 4.3. Patterning in two dimensions

Following other studies, we have treated somitogenesis as a one-dimensional process along the AP axis of the PSM. To validate this, we now consider whether the model is still capable of forming somites when extended to two dimensions.

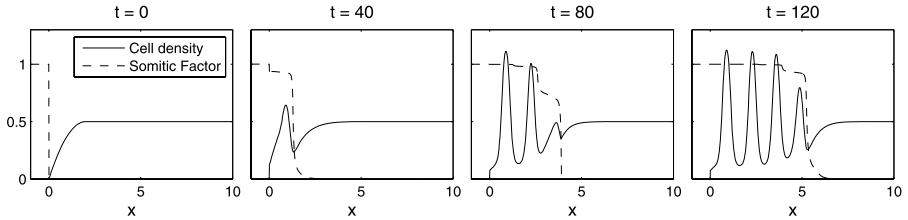


**Fig. 10** Solutions of the model (2, 6) with initial conditions in which  $n$  increases gradually from 0 to  $N$ , rather than being a step function. The first somite is of a similar size to the others, in contrast to solutions when  $n(x, t = 0)$  is a step function (see, for example, Fig. 6). Specifically, we use  $n = x(1 - x/4)N$  for  $0 < x < 2$ , with  $n = 0$  for  $x < 0$  and  $n = N + \Phi(x)$  for  $x > 2$ ;  $\Phi(x)$ . The equations were solved on  $-10 < x < 10$  with numerical details, chemical initial conditions, and parameter values as in Fig. 6, with  $N = 0.5$ .

We consider a thin rectangular domain representing a posterior–anterior/medial–lateral cross-section of one side of the PSM. The extension of Eqs. (2) to 2D is trivial, while Eq. (6) for the cells is replaced with its equivalent 2D form, derived in Armstrong et al. (2006).

$$\frac{\partial u}{\partial t} = \frac{(u + \mu v)^2}{\gamma + \kappa u^2} \chi_u(x, t) - \frac{u}{\kappa}, \quad (9a)$$

$$\frac{\partial v}{\partial t} = \frac{\chi_v(x, t)}{\epsilon + u} - v + D \nabla^2 v, \quad (9b)$$

$$\frac{\partial n}{\partial t} = \nabla \cdot \left[ D_n \nabla n - \alpha u n \int_{\theta=0}^{2\pi} \int_{r_0=0}^r u(\underline{x} + r_0 \underline{\eta}, t) f(n(\underline{x} + r_0 \underline{\eta}, t)) r_0 \underline{\eta} dr_0 d\theta \right]. \quad (9c)$$

Here,  $\underline{x} = (x, y)$ ,  $\underline{\eta} = (\cos \theta, \sin \theta)$ , and  $\chi_u$  and  $\chi_v$  are as in model (2). This extends the 1D formulation naturally by assuming that the adhesive component of cell movement at  $\underline{x}$  derives from a summation of the adhesive forces generated through interactions with cells at  $\underline{x} + r_0 \underline{\eta}$  within a circular sensing region of radius  $r$ . The function  $f$  is assumed to take the same form as for the 1D model. Initial conditions are directly extended from the 1D model.

The results from 2D simulations are displayed in Fig. 11 (see also the accompanying movie at <http://www.ma.hw.ac.uk/~painter/somites/movie.html>). The model predicts the formation of discrete circular somites at locations determined by the chemical model. As for the 1D case, correct patterning depends on the initial cell density and wavespeed, and coarsening of the pattern arises under inappropriately chosen parameters (data not shown). These results confirm that the 1D simplification of the problem is valid.

## 5. Further model expansion: anterior–posterior differentiation

Shortly after the formation of a somite, it differentiates into separate anterior and posterior halves (Saga and Takeda, 2001; Pourquié, 2001). We can model this by considering the two halves to be composed of two cell populations with distinct adhesive properties.

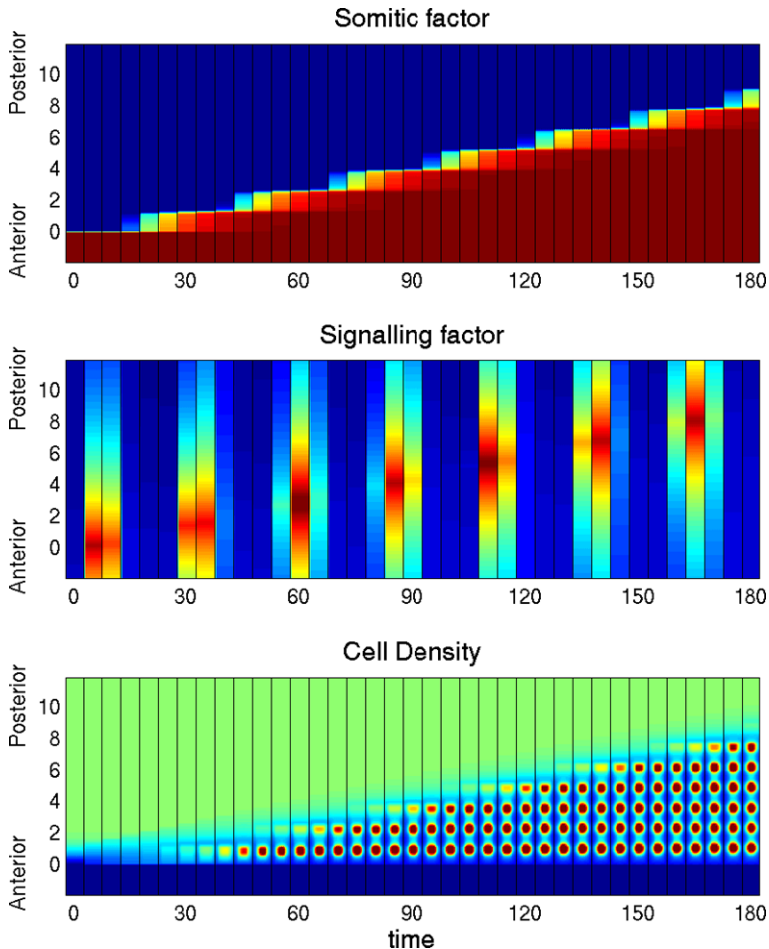


**Fig. 11** Simulations of the 2D model (9) showing the periodic formation of circular somites at the locations and times predicted by the chemical model. Simulations are conducted on the domain  $(x, y) \in [-10, 10] \times [-0.6, 0.6]$  with initial conditions that are independent of  $y$  and are given by (3) for the chemicals and by  $n = x(1 - x/4)N$  for  $0 < x < 2$ , with  $n = 0$  for  $x < 0$  and  $n = N$  for  $x > 2$ . Note that for the above simulations noise was not added to the initial cell density, however, the addition of spatial noise varying with both  $x$  and  $y$  did not alter the dynamics (data not shown). The parameter values are as for the 1D case, i.e., as in Fig. 6, with  $N = 0.25$ . The color scale from dark to light (blue to red in the color version of the figure) indicates increasing cell density/chemical concentration. Note that the fine resolution required for approximation of the integral in 2D necessitated a simulation time of 16 days on a Dual Xeon 3.2 GHz processor. An animation corresponding to this figure is available at <http://www.ma.hw.ac.uk/~painter/somites/movie.html>. Color version of the figure is available at <http://www.ma.hw.ac.uk/~painter/somites/fig1colour.eps> (Color figure online.)

The hypothesis of two distinct populations is a modelling assumption, yet not unreasonable given the highly dynamic and variable gene expression in the PSM prior to somite formation (e.g., Saga and Takeda, 2001; Pourquié, 2001). We thus extend the cell-cycle model further, introducing a pair of coupled equations describing the two interacting cell

populations. In this way, we can model both somite formation and cell sorting within the somites.

We denote the densities of the two cell types  $n_1(x, t)$  and  $n_2(x, t)$ . We assume that they respond in the same way to the chemicals, and interact with one another through cell–cell adhesion. Crucially, we assume that cells are more adhesive to other cells of their own type than to cells of the other type. The dimensionless equations for the cells are

$$\begin{aligned} \frac{\partial n_1(x, t)}{\partial t} = D \frac{\partial^2 n_1(x, t)}{\partial x^2} \\ - \frac{\partial}{\partial x} \left[ u(x, t) n_1(x, t) (\alpha K_1(u, n_1, n_2) + \beta K_2(u, n_1, n_2)) \right], \end{aligned} \quad (10a)$$

$$\begin{aligned} \frac{\partial n_2(x, t)}{\partial t} = D \frac{\partial^2 n_2(x, t)}{\partial x^2} \\ - \frac{\partial}{\partial x} \left[ u(x, t) n_2(x, t) (\alpha K_2(u, n_1, n_2) + \beta K_1(u, n_1, n_2)) \right], \end{aligned} \quad (10b)$$

where

$$\begin{aligned} K_i(u, n_1, n_2) = \int_{-r}^r u(x + x_0, t) n_i(x + x_0, t) (2 - n_1(x + x_0, t) \\ - n_2(x + x_0, t)) \omega(x_0) dx_0 \end{aligned}$$

( $i = 1, 2$ ). This two population expansion of (6) is again based on the work of Armstrong et al. (2006), but with adhesion dependent on the somitic factor  $u$ . The positive parameters  $\alpha$  and  $\beta$  are the self-population and cross-population adhesion coefficients, respectively; for simplicity, we assume that the two cell populations have the same self-adhesion coefficient, though this is not essential. Also for simplicity, we assume that  $n_1(x, t = 0)$  and  $n_2(x, t = 0)$  are both 0 for  $x < 0$ , with  $n_i(x, 0) = N/2 + \Phi_i(x)$  for  $x > 2$  ( $i = 1, 2$ ). As for the one-population simulations,  $\Phi_1(\cdot)$  and  $\Phi_2(\cdot)$  are very small levels of noise. In the one-population model, this noise did not play any significant role, but here it is crucial, since it breaks the symmetry between  $n_1$  and  $n_2$ . In  $0 < x < 2$ , we take  $n_1$  and  $n_2$  to increase gradually from 0 to  $N/2$ , so that the first somite has an appropriate size (see the legend of Fig. 12 for details).

In the one-population case, we derived the approximate constraint (8) on  $\alpha$  and  $N$  by requiring the fastest growing linear mode to have wavelength 1. For the amended model (10), linear stability analysis yields a corresponding constraint on  $\alpha$ ,  $\beta$  and  $N$ :

$$\frac{1}{2}(\alpha + \beta)N(1 - N)r \sin(2\pi r) = \pi D_n. \quad (11)$$

We solve the new model numerically, using the same method as for the one population case (described in the Appendix). Provided that  $\alpha$  and  $\beta$  approximately satisfy condition (11), the model predicts the formation of cellular aggregates with a spacing appropriate for somites, as in the one-population case. Moreover, provided that  $\alpha > \beta \neq 0$ , the model can also replicate the observed sorting of the anterior and posterior cell types; a typical solution is illustrated in Fig. 12 while an animation corresponding to this figure is available at <http://www.ma.hw.ac.uk/~painter/somites/movie.html>. This is due to

the relative strengths of self-population and cross-population adhesion, and develops despite the initial conditions being essentially the same for the two populations. The initial somite generally develops in a slightly irregular manner, depending on the noise in the initial conditions: in the simulation in Fig. 12, a pattern resembling “encapsulation” is observed for the first somite, rather than distinct anterior–posterior halves. In all subsequent somites, distinct anterior–posterior somites develop with the same ordering maintained throughout. This is because as an aggregate develops in one cell population, cell sorting leads to the formation of a smaller aggregate of the other population on the anterior side. This establishes the  $n_1$ – $n_2$  ordering in the next somite to form. Without any cell population bias in the random initial data, the anterior–posterior compartmentalization of each somite forms as either  $n_1$ – $n_2$ : $n_1$ – $n_2$ : $n_1$ – $n_2$ :... or  $n_2$ – $n_1$ : $n_2$ – $n_1$ : $n_2$ – $n_1$ :... with equal likelihood. To the best of our knowledge, our model is the first to reproduce the fundamental feature of anterior–posterior differentiation within somites using explicit variables for cell populations (rather than prepatterned chemicals, such as in Meinhardt’s (1986) model).

We have also investigated the robustness of the mechanism for anterior-patterning with respect to the ratio between the self- and cross-adhesion parameters (Fig. 13). We observe that clearly defined and partitioned somites only arise when  $\alpha/\beta$  is relatively large, and also  $\beta$  not very small (Figs. 13(c)–(e)). For  $\alpha/\beta \lesssim 1$  (i.e., larger cross adhesion), the two populations remain mixed and are unable to separate into distinct anterior–posterior segments can occur (Figs. 13(a) and (b)). For small cross population adhesion ( $\alpha/\beta \gtrsim 10$ ), the cross-adhesion is ineffective in maintaining the border between the anterior and posterior segments and the somite splinters into 2 distinct clusters (e.g., Fig. 13(f)).

## 6. Discussion

The main objective of this paper was to understand the conditions under which inclusion of cellular dynamics in an existing chemical model for somitic patterning predicts actual somite formation. To this end, the model of Collier et al. (2000) was augmented with an integro-partial differential equation that describes an adhesive cell population, adapting the method described in Armstrong et al. (2006). In the formulation of the model, the adhesive strength between the cells depends on the output from the chemical model, thus assuming that the somitic factor in Collier et al. (2000) acts as a precursor to increased cell–cell adhesion. The correct aggregation of cells into somites was shown to occur, but only under specific parameter constraints. Otherwise, somites formed too slowly and/or underwent a coarsening phenomena in which multiple somites coalesced. These results give experimentally testable conditions under which the chemical model must operate to correctly generate somites.

Simulations indicated that for appropriate parameters, regularly spaced somites were found to be stable over long time periods: the animation corresponding to Fig. 6,  $N = 0.3$  (at <http://www.ma.hw.ac.uk/~painter/somites/movie.html>) shows regular somite formation over a simulation timeframe corresponding to 18 somites. Nevertheless, over longer time periods, a coarsening of the pattern will still occur and the degree/speed of coarsening depends on the initial cell density (cf. Fig. 8). Coarsening is a well-documented phenomenon in cell movement models without cell kinetics (e.g., Hillen and Painter, 2001) and here it takes place over a much longer timescale than the formation of a somite. Somites

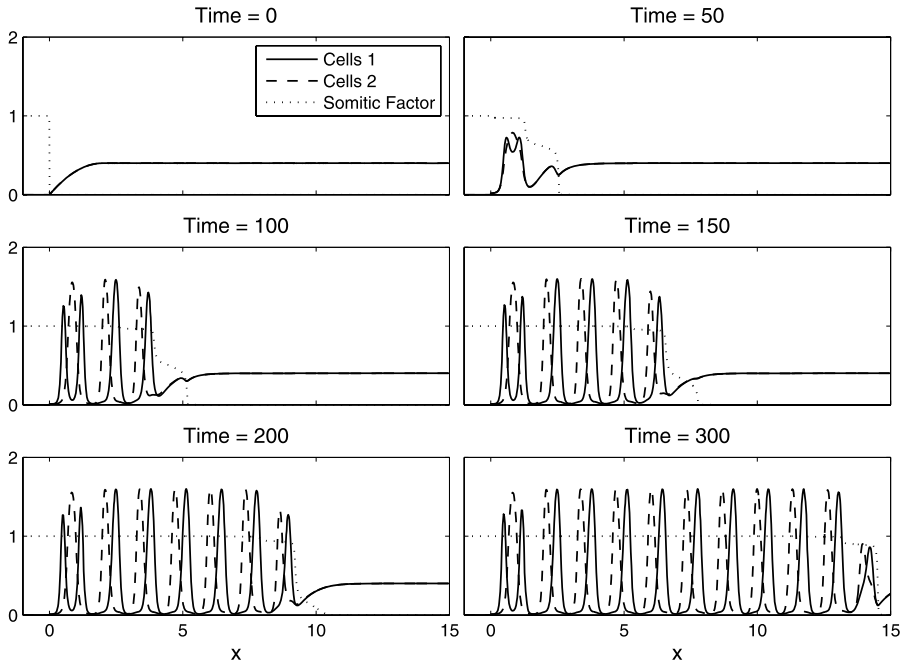


**Fig. 12** Solutions of the model (2, 10) showing the development of somites that are differentiated into separate anterior and posterior halves. The dotted line shows the wavefront of the somitic factor. Cell parameters are  $D_i = 0.02$ ,  $r = 0.25$ ,  $N = 0.8$  with  $\alpha = \frac{4\pi}{5}$ ,  $\beta = \frac{\pi}{5}$  chosen to satisfy (11); chemical parameters are as in Fig. 6. The initial population densities are  $n_i = 0$  when  $x < 0$ ,  $n_i = x(1 - x/4)N + \Phi_i(x)$  on  $0 < x < 2$ , and  $n_i = N + \Phi_i(x)$  for  $x > 2$  ( $i = 1, 2$ ). As in the one-population simulations,  $\Phi_1(x)$  and  $\Phi_2(x)$  are small levels of noise that are added at each grid element in the numerical scheme, chosen randomly from a uniform distribution between  $\pm 5 \times 10^{-4}$ . In this case, the noise plays an important role by breaking the symmetry between  $n_1$  and  $n_2$ . Note that the first somite forms slightly irregularly, but sets an  $n_1 - n_2$  ordering that is maintained in all subsequent somites, as explained in the main text. The equations were solved numerically as described in the Appendix, on the domain  $-10 < x < 20$  (only the relevant part of which is illustrated) subject to zero flux boundary conditions and a spatial discretization of  $\Delta x = 0.0125$ . An animation corresponding to this figure is available at <http://www.ma.hw.ac.uk/~painter/somites/movie.html>.

are transient embryonic structures and additional factors may come into play during formation and maintenance of the boundaries between somites. Certainly, *in vivo*, signaling networks such as Delta–Notch are involved in marking the initial borders between somites (e.g., Pourquié, 2001) and the presence of fibronectin at the boundaries (Duband et al., 1987) indicates that cell–ECM interactions also play an important role. (For a recent review of somite border formation, see Kulesa et al., 2007.) An important avenue for future research would be to extend the model to incorporate these additional factors and evaluate their contribution to robust somite development.

In the model described here, the cell equation is decoupled from the chemical equations: this simple assumption allowed us to investigate the additional constraints imposed on the signaling model by incorporation of cell kinetics. In reality, it is likely that feedback would occur from the cells to the signaling network, for example, through cellular regu-

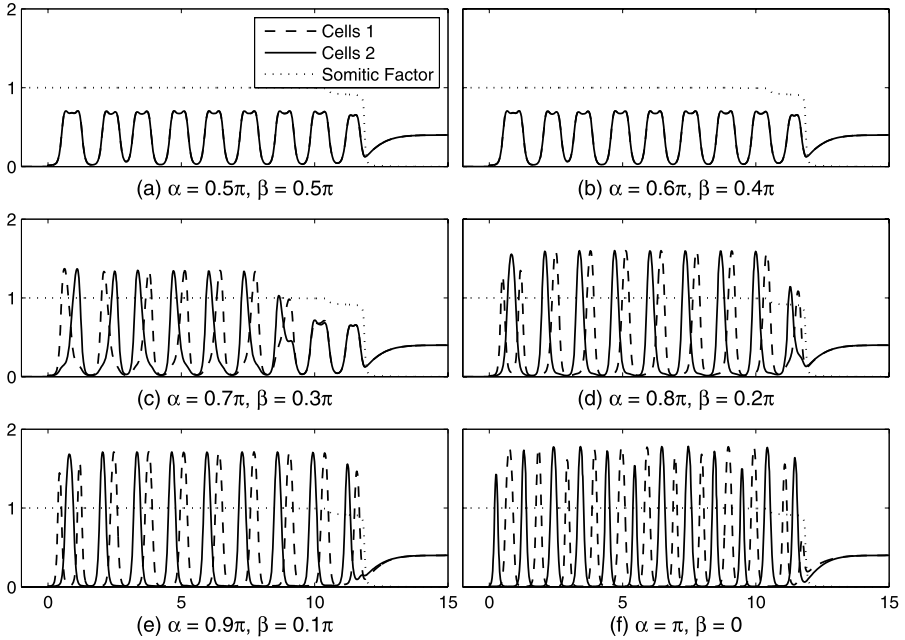


**Fig. 13** Solutions of the model (2, 10) demonstrating the robustness of the anterior–posterior patterning mechanism with respect to the ratio  $\alpha : \beta$ . Model parameters are the same as for Fig. 12 except for  $\alpha$  and  $\beta$ , the ratio of which is changed while maintaining (11). Profiles for the cells and somitic factor are shown at  $t = 250$  for (a)  $\alpha = 0.5\pi$ ,  $\beta = 0.5\pi$ , (b)  $\alpha = 0.6\pi$ ,  $\beta = 0.4\pi$ , (c)  $\alpha = 0.7\pi$ ,  $\beta = 0.3\pi$ , (d)  $\alpha = 0.8\pi$ ,  $\beta = 0.2\pi$ , (e)  $\alpha = 0.9\pi$ ,  $\beta = 0.1\pi$  and (f)  $\alpha = \pi$ ,  $\beta = 0$ . Correct partitioning of the somites is found to occur for cases (c), (d) and (e). For (a) and (b),  $\alpha$  and  $\beta$  are similar in size and the two populations remain uniformly dispersed throughout the somite. For very small or zero  $\beta$  (case (f)), the single somite splinters into two separate aggregations. Initial data and other numerical details are as in Fig. 12.

lation of chemical kinetics. The impact of different types of regulation on the robustness of patterning is an obvious area for future research. Another natural area for future study is the inclusion of intermediate signaling steps between somitic factor production and increased cell adhesion; we anticipate that this would extend the delay between prepattern expression and actual somite formation to be closer to that found experimentally. We further note that we have considered the effect of introducing cell adhesion into only one of many chemical models of somitic patterning. It is anticipated that its incorporation into those models drawn from the Collier et al. (2000) model (for example, those of Baker et al. 2006a, 2006b) would give rise to very similar results to those presented here; however, an investigation into its effect on other models of somitogenesis (e.g., the reaction–diffusion model of Meinhardt, 1986) remains unexplored.

The distribution of various types of cell–cell adhesion molecule within the PSM has led to the hypothesis that differential adhesion may play some role in the differentiation of somites into anterior and posterior compartments (e.g., Stern and Keynes, 1987). We further extended the model by considering two cell subpopulations with distinct adhesive properties. Our model demonstrated that differential adhesion alone is able to generate the correct AP patterning of the somites, even with an initially almost-homogeneous mix-

ing of the two cell populations. Of course, an anterior–posterior division of presumptive somites is observed within the PSM even prior to somite formation, thereby suggesting that a spatial separation of various cell populations may arise even prior to the epithelialization of the somite. The coupling of this prepatterning prior to somite formation with differential adhesion during their development would provide a robust mechanism for generating the AP patterning.

Following epithelialization, somites undergo further pattern formation. The ventral–medial portion forms the sclerotome, the cells of which ultimately regain mesenchymal characteristics and disperse to form the vertebral chondrocytes. The lateral portion of the somite also disperses, giving rise to the limb musculature. The remaining dorsal–lateral portion forms the dermomyotome which undergoes further differentiation into the dermatome (which forms the dermis) and myotome (which gives rise to muscle cells). This later stage of somitogenesis has not been considered here and extension of our model to investigate this process would require the incorporation of additional factors, such as signaling from the surrounding embryonic structures (Bothe et al., 2007).

A number of simulations were conducted to investigate patterning in higher dimensions. Simulations in 2D revealed periodic formation of regularly spaced circular somites at the locations predicted by the chemical model. An interesting area for further investigation is to understand how the geometry of the cell sensing region contributes to the shape of the somite. In the simulations here, we have focused exclusively on the logical case of a circular sample region, yet different geometries may also be plausible: for example, if cells become stretched along a particular axis or extend filopodia in specific directions. The time-consuming nature of the 2D simulations will necessitate the development of novel numerical schemes to investigate these questions in detail.

Cell–cell adhesion and other forms of cellular movement are critical in many processes of embryonic growth including gastrulation, somitogenesis, skeletal patterning and the development of the nervous system. The results presented here stress how the incorporation of cellular dynamics can place additional constraints on the conditions under which chemical-only models can correctly predict embryonic patterning, as well as demonstrating additional contributions to the pattern formation process arising from cellular dynamics.

## Appendix A: Numerical Methods

Our numerical solutions of (2), (2, 6), and (2, 10) use a finite volume scheme. The general approach in this type of scheme is to discretize the domain into grid points; we have used a uniform grid spacing  $\Delta x$  although a nonuniform grid could also be used. One then considers the domain to be composed of regions whose boundaries lie halfway between the grid points. The flux between the regions is then calculated, enabling the change in concentration or density within a region to be found as the total flux entering minus the total flux leaving. The concentration at each grid point is then approximated by averaging the concentration within each region. This results in a system of ordinary differential equations which can be solved by an appropriate integration technique. Since the flux over the right-hand boundary of region  $i$  is always equal to the flux over the left-hand boundary of region  $i + 1$ , a finite volume scheme ensures mass conservation.

Although our equations are posed mathematically on an infinite domain, numerical solution requires a (large) finite domain, and in each variation of the model we employ zero flux boundary conditions. The only difficulty in implementation of these boundary conditions lies in the adhesion term in the cell equation when the integral contains a boundary point. In this case, we simply assume that there are no cells located outside the domain. Since the adhesion term only allows cells to move to regions with positive cell density, this prevents movement across the boundary. The direction of movement of cells near the boundary then tends to be toward the center of the domain. However, in practice, we choose the domain size sufficiently large that over the time period of interest, activity is confined to a central region, and the boundary conditions have a negligible impact on the solution.

### A.1 Cell-cycle model

In the chemical model, we use the above technique and employ a central difference scheme to find the diffusive flux at the cell boundaries. To avoid problems associated with the discontinuities in (2), we follow Baker et al. 2006a, 2006b and approximate the Heaviside functions by tanh functions in the numerical scheme. Specifically, we use  $\chi_u = \frac{1}{2}(1 + \tanh[1000(x_1 - x)])$  and  $\chi_v = \frac{1}{2}(1 + \tanh[1000(x_2 - x)])$ .

The large systems of ODEs generated through the method of lines approach necessitates an efficient yet reliable time discretization: here we have employed the ROWMAP stiff systems integrator (Weiner et al., 1997, see also Gerisch and Chaplain, 2008; Gerisch, 2008). To control accuracy of the numerical method, simulations have been compared with those obtained through an explicit method (forward Euler) and for a range of  $\Delta x$ .

### A.2 Adding adhesive cells to the model

For (6) and (10), we calculate the diffusive fluxes using a central difference scheme and the adhesive fluxes using a first order upwinding scheme. The integral within the advection term is calculated directly by summing over the enclosed points. As above, the system of ODEs derived through the spatial discretization is integrated in time using ROWMAP. The numerics have been compared against those using an explicit scheme (forward Euler method for the chemical equations (2), and an explicit trapezoidal method for the cell equation(s) (6) or (10)) and across a range of spatial discretizations ( $\Delta x$ ). As for the cell cycle model alone, we approximate the Heaviside functions in (2) by tanh functions.

### A.3 2D numerics

The two-dimensional equations (9) were solved numerically using a method of lines approach similar to that described for the 1D numerics. The spatial terms were discretized, using a central difference scheme for the diffusion terms and an upwind method for the advective component. The integral term in 2D was approximated using the approach described in Armstrong et al. (2006). Briefly, we first discretized the radial component to give concentric rings of radius  $r_0$ ,  $0 < r_0 < r$ . We then discretized each circular surface and employed linear interpolation from the surrounding grid points to calculate the densities/concentrations at the surface. The time integration was again performed using the ROWMAP stiff systems integrator. The boundary conditions are taken to be zero flux for

both cells and chemical; for cells located near the boundaries (i.e., within distance  $r$ ), we assume zero contribution to the integral term in Eq. (9) from positions outside the domain. This effectively proposes that there are no cells outside the PSM contributing to the adhesive force exerted on those within it.

## References

- Armstrong, N.J., Painter, K.J., Sherratt, J.A., 2006. A continuum approach to modelling cell–cell adhesion. *J. Theor. Biol.* 243, 98–113.
- Bagnall, K.M., Higgins, S.J., Sanders, E.J., 1989. The contribution made by cells from a single somite to tissues within a body segment and assessment of their integration with similar cells from adjacent segments. *Development* 107, 931–943.
- Baker, R.E., Schnell, S., Maini, P.K., 2006a. A clock and wavefront mechanism for somite formation. *Dev. Biol.* 293, 116–126.
- Baker, R.E., Schnell, S., Maini, P.K., 2006b. A mathematical investigation of a clock and wavefront model for somitogenesis. *J. Math. Biol.* 52, 458–482.
- Baker, R.E., Schnell, S., Maini, P.K., 2008. Mathematical models for somite formation. *Curr. Top. Dev. Biol.* 81, 183–203.
- Bothe, I., Ahmed, M.U., Winterbottom, F.L., von Scheven, G., Dietrich, S., 2007. Extrinsic versus intrinsic cues in avian paraxial mesoderm patterning and differentiation. *Dev. Dyn.* 236, 2397–2409.
- Cheney, C.M., Lash, J.W., 1984. An increase in cell–cell adhesion in the chick segmental plate results in a meristic pattern. *J. Embryol. Exp. Morphol.* 79, 1–10.
- Collier, J.R., McInerney, D., Schnell, S., Maini, P.K., Gavaghan, D.J., Houston, P., Stern, C.D., 2000. A cell cycle model for somitogenesis: Mathematical formulation and numerical simulation. *J. Theor. Biol.* 207, 305–316.
- Cooke, J.R., Zeeman, E.C., 1976. A clock and wavefront model for control of the number of repeated structures during animal morphogenesis. *J. Theor. Biol.* 58, 455–476.
- Dale, K.J., Pourquié, O., 2000. A clock-work somite. *Bioessays* 22, 72–83.
- Duband, J.L., Dufour, S., Hatta, K., Takeichi, M., Edelman, G.M., Thiery, J.P., 1987. Adhesion molecules during somitogenesis in the avian embryo. *J. Cell. Biol.* 104, 1361–1374.
- Dubrulle, J., McGrew, M.J., Pourquié, O., 2001. FGF signaling controls somite boundary position and regulates segmentation clock control of spatiotemporal Hox gene activation. *Cell* 106, 219–232.
- Dubrulle, J., Pourquié, O., 2004a. Coupling segmentation to axis formation. *Development* 131, 5783–5793.
- Dubrulle, J., Pourquié, O., 2004b. *fgf8* mRNA decay establishes a gradient that couples axial elongation to patterning in the vertebrate embryo. *Nature* 427(6973), 419–422.
- Foty, R.A., Steinberg, M.S., 2004. Cadherin-mediated cell–cell adhesion and tissue segregation in relation to malignancy. *Int. J. Dev. Biol.* 48, 397–409.
- Foty, R.A., Steinberg, M.S., 2005. The differential adhesion hypothesis: A direct evaluation. *Dev. Biol.* 278, 255–263.
- Gerisch, A., 2008. On the approximation and efficient evaluation of integral terms in PDE models of cell adhesion. Submitted.
- Gerisch, A., Chaplain, M., 2008. Mathematical modelling of cancer cell invasion of tissue: local and non-local models and the effect of adhesion. *J. Theor. Biol.* 250, 684–704.
- Glazier, J.A., Zhang, Y., Swat, M., Zaitlen, B., Schnell, S., 2008. Coordinated action of N-CAM, N-cadherin, EphA4, and ephrinB2 translates genetic prepattens into structure during somitogenesis in chick. *Curr. Top. Dev. Biol.* 81, 205–247.
- Grima, R., Schnell, S., 2007. Can tissue surface tension drive somite formation? *Dev. Biol.* 307, 248–257.
- Hatta, K., Takagi, S., Fujisawa, H., Takeichi, M., 1987. Spatial and temporal expression pattern of N-cadherin cell adhesion molecules correlated with morphogenetic processes of chicken embryos. *Dev. Biol.* 120, 215–227.
- Hillen, T., Painter, K.J., 2001. A parabolic model with bounded chemotaxis—prevention of overcrowding. *Adv. Appl. Math.* 26, 280–301.
- Horikawa, K., Radice, G., Takeichi, M., Chisaka, O., 1999. Adhesive subdivisions intrinsic to the epithelial somites. *Dev. Biol.* 215, 182–189.

- Kimura, Y., Matsunami, H., Inoue, T., Shimamura, K., Uchida, N., Ueno, T., Miyazaki, T., Takeichi, M., 1995. Cadherin-11 expressed in association with mesenchymal morphogenesis in the head, somite, and limb bud of early mouse embryos. *Dev. Biol.* 169, 347–358.
- Kulesa, P.M., Schnell, S., Rudloff, S., Baker, R.E., Maini, P.K., 2007. From segment to somite: segmentation to epithelialization analyzed within quantitative frameworks. *Dev. Dyn.* 236, 1392–1402.
- Lash, J.W., Linask, K.K., Yamada, K.M., 1987. Synthetic peptides that mimic the adhesive recognition signal of fibronectin: differential effects on cell–cell and cell–substratum adhesion in embryonic chick cells. *Dev. Biol.* 123, 411–420.
- Lewis, J., Ozbudak, E.M., 2007. Deciphering the somite segmentation clock: beyond mutants and morphants. *Dev. Dyn.* 236, 1410–1415.
- Linask, K.K., Ludwig, C., Han, M.D., Liu, X., Radice, G.L., Knudsen, K.A., 1998. N-cadherin/catenin-mediated morphoregulation of somite formation. *Dev. Biol.* 202, 85–102.
- McGrew, M.J., Dale, K., Fraboulet, S., Pourquié, O., 1998. The *lunatic Fringe* gene is a target of the molecular clock linked to somite segmentation in avian embryos. *Curr. Biol.* 8, 979–982.
- McInerney, D., Schnell, S., Baker, R.E., Maini, P.K., 2004. A mathematical formulation for the cell-cycle model in somitogenesis: Analysis, parameter constraints and numerical solutions. *Math. Med. Biol.* 21, 85–113.
- Meinhardt, H., 1986. Models of segmentation. In: *Somites in Developing Embryos*, pp. 179–189. Plenum, New York.
- Ostrovsky, D., Cheney, C.M., Seitz, A.W., Lash, J.W., 1983. Fibronectin distribution during somitogenesis in the chick embryo. *Cell. Differ.* 13, 217–223.
- Palmeirim, I., Henrique, D., Ish-Horowicz, D., Pourquié, O., 1997. Avian *hairy* gene expression identifies a molecular clock linked to vertebrate segmentation and somitogenesis. *Cell* 91, 639–648.
- Pourquié, O., 2001. Vertebrate somitogenesis. *Ann. Rev. Cell. Dev. Biol.* 17, 311–350.
- Primmitt, D., Norris, W., Carlson, G., Keynes, R., Stern, C., 1989. Periodic segmental anomalies induced by heat shock in the chick embryo are associated with the cell cycle. *Development* 105, 119–130.
- Primmitt, D.R., Stern, C.D., Keynes, R.J., 1988. Heat shock causes repeated segmental anomalies in the chick embryo. *Development* 104, 331–339.
- Saga, Y., Takeda, H., 2001. The making of the somite: molecular events in vertebrate segmentation. *Nat. Rev. Genet.* 2, 835–845.
- Schnell, S., Maini, P.K., McInerney, D., Gavaghan, D.J., Houston, P., 2002. Models for pattern formation in somitogenesis: A marriage of cellular and molecular biology. *C. R. Biol.* 325, 179–189.
- Steinberg, M.S., 1962. On the mechanism of tissue reconstruction by dissociated cells, III. Free energy relations and the reorganization of fused, heteronomic tissue fragments. *PNAS* 48, 1769–1776.
- Stern, C.D., Keynes, R.J., 1987. Interactions between somite cells: the formation and maintenance of segment boundaries in the chick embryo. *Development* 99, 261–272.
- Stern, C.D., Fraser, S.E., Keynes, R.J., Primmitt, D.R.N., 1988. A cell lineage analysis of segmentation in the chick embryo. *Development* 104S, 231–244.
- Takeichi, M., 1988. The cadherins: cell–cell adhesion molecules controlling animal morphogenesis. *Development* 102, 639–655.
- Weiner, R., Schmitt, B., Podhaisky, H., 1997. Rowmap—a row-code with Krylov techniques for large stiff odes. *Appl. Num. Math.* 25, 303–319.